Modeling of quasi-phase-matched cavity-enhanced second-harmonic generation

C. Mas Arabí,[1] P. Parra-Rivas,[1] C. Ciret,[2] S. P. Gorza,[1] and F. Leo[1]
[1]*OPERA-Photonique CP 194/5, Université libre de Bruxelles (ULB), Av. F.D. Roosvelt 50, B-1050 Bruxelles, Belgium*
[2]*Laboratoire de Photonique d'Angers EA 4464, Université d'Angers, 2 Bd. Lavoisier, 49000 Angers, France*

(Received 12 December 2019; accepted 12 March 2020; published 14 April 2020)

We propose a mean-field model to describe second-harmonic generation in a resonator made of a material with zinc-blende crystalline structure. The model is obtained through an averaging of the propagation equations and boundary conditions. It considers the phase-mismatched terms, which act as an effective Kerr effect. We analyze the impact of the different terms on the steady state solutions, highlighting the competition between nonlinearities.

DOI: 10.1103/PhysRevA.101.043818

I. INTRODUCTION

Frequency conversion plays an important role in the production of optical sources [1] or in many technological applications in biophotonics [2] and quantum information [3]. Nanometric scale waveguides are particularly well suited for nonlinear optics as they allow confining light down to subwavelength scales, strongly increasing light-matter interactions. While many different materials have been used for integrated frequency conversion, the ones with a stronger quadratic response, such as III-V semiconductors and lithium niobate, have recently attracted increasing attention [4,5]. Ring resonators in particular have allowed for record conversion efficiencies as both the power and the interaction length are greatly enhanced [6]. Harnessing these resonators for efficient frequency conversion requires to fulfill a phase matching condition [7]. Quasi-phase-matching (QPM) is attractive because it allows the coupling between fundamental modes, maximizing the effective nonlinearity. While most often engineered by poling [8,9] or orientation patterning [10], QPM also naturally occurs in some crystals such as BBO [11,12] and III-V semiconductors [13,14]. In the latter, the sign of the effective nonlinearity changes every quarter round trip, because of the $\bar{4}$ symmetry of the material. The propagation geometry is hence equivalent to that in a poled medium with a πR period, where R is the radius of the resonator, and similar nonlinear dynamics is to be expected. In the case of second-harmonic (SH) generation, QPM is known to induce an effective Kerr nonlinearity through cascaded three-wave mixing [15]. Because there are mismatched nonlinear interactions, a fraction of the SH wave gets converted back to the pump with a shifted, power-dependent phase [16]. This effect allows engineering competing nonlinearities [17] and can be used for pulse compression [18] as well as ultrabroadband light generation [19]. However, despite potential applications, the impact of cascaded nonlinearities on the dynamics of QPM resonators is, to the best of our knowledge, still poorly understood.

In this paper, we derive a mean-field model that describes SH generation in a passive quasi-phase-matched III-V-on-insulator cavity. We investigate the impact of cascaded three-wave mixing and find that it can affect the conversion efficiency in some circumstances.

While our analysis focuses on III-V semiconductor rings, we stress that it can readily be generalized to any resonator with a periodic modulation of the nonlinear susceptibility and/or refractive index [9,11].

The paper is organized as follows. In Sec. II, we describe light propagation in a bent waveguide and study the impact of the curvature on the nonlinear coefficient. In Sec. III, we derive a mean-field equation which models the propagation in a III-V resonator and takes into account the phase-mismatched terms. Section IV is devoted to the study of stationary solutions. Finally, in Sec. V, we summarize our results and discuss their implications on the design of cavity-enhanced SH generation.

II. DESCRIPTION OF THE PROPAGATION IN A RESONATOR

The resonator under study is sketched in Fig. 1. It is made of indium gallium phosphide (InGaP), grown in the [010] direction, bonded on silica [20,21].

The electric field $\mathbf{E}(\mathbf{r}_\perp, \phi, \omega)$ can be expressed as a sum of two modes:

$$\mathbf{E} = a(\phi)\frac{\mathbf{e}_a(\mathbf{r}_\perp, \omega_0)}{\sqrt{N_a}} e^{i(\beta_a R\phi - \omega_0 t)} + b(\phi)\frac{\mathbf{e}_b(\mathbf{r}_\perp, 2\omega_0)}{\sqrt{N_b}} e^{i(\beta_b R\phi - 2\omega_0 t)}, \quad (1)$$

where, β_a, and β_b are the propagation constants of the fundamental wave (FW) and SH, ω_0 is the frequency of the FW, $|a(\phi)|^2$ and $|b(\phi)|^2$ represent the power carried by the FW and SH modes respectively, $\mathbf{e_a}$ and $\mathbf{e_b}$ are the corresponding vector mode distributions of the electric field, and ϕ is the azimuthal angle. N_j are the normalization constants provided by the following expression:

$$\mathrm{Re}\left(\int \mathbf{e}_i(\mathbf{r}_\perp, \omega) \times \mathbf{h}_j^*(\mathbf{r}_\perp, \omega) \cdot \mathbf{dS}\right) = 2N_i\delta_{ij}, \quad (2)$$

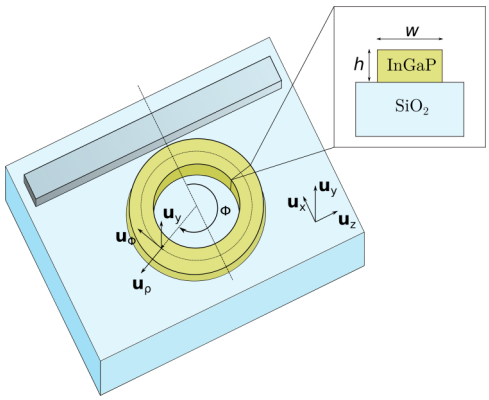

FIG. 1. Sketch of the considered resonator. The coordinates $(\mathbf{u}_x, \mathbf{u}_y, \mathbf{u}_z)$ stand for the crystal axis while $(\mathbf{u}_\rho, \mathbf{u}_y, \mathbf{u}_\phi)$ refer to the cylindrical basis of the resonator. The inset shows the transverse structure of the ring that is composed of a rectangular waveguide of height h and width w.

where δ_{ij} is the Kronecker delta and $\mathbf{h}$ is the vector mode distribution of the magnetic field. The field amplitudes are governed by the following system of ordinary differential equations:

$$\begin{aligned} R^{-1}\frac{da}{d\phi} &= -\frac{\alpha_a}{2}a + i\kappa^*(\phi)ba^*e^{-i\Delta\beta R\phi}, \\ R^{-1}\frac{db}{d\phi} &= -\frac{\alpha_b}{2}b + i\kappa(\phi)a^2e^{i\Delta\beta R\phi}, \end{aligned} \tag{3}$$

where $\Delta\beta = 2\beta_a - \beta_b$ corresponds to the wave-vector mismatch, α_a, α_b are the loss coefficients associated to the propagation, and $\kappa(\phi)$ is the nonlinear coefficient. To focus on the effects of cascaded three-wave mixing, we neglect higher-order nonlinearities.

The value of $\kappa(\phi)$ is determined by the symmetries of the crystalline structure and the propagation direction. In the case of materials with $\bar{4}3m$ structure, the only nonzero tensorial element of the electric susceptibility ($\chi^{(2)}_{ijk}$) is $\chi^{(2)}_{xyz}$ with $x \neq y \neq z$. The value of $\chi^{(2)}_{xyz}$ has been measured for indium gallium phosphide to be as high as 220 pm/V around 1550 nm [22]. When the propagation direction is aligned with a crystallographic axis, the effective nonlinearity (κ) reads [21]

$$\kappa = \frac{\epsilon_0\omega_0}{2N_a\sqrt{N_b}}\int_G \chi^{(2)}_{xyz}\left(e_b^{*x}e_a^y e_a^z + e_b^{*y}e_a^x e_a^z + e_b^{*z}e_a^x e_a^y\right)dS, \tag{4}$$

where $e_a^k(e_b^k)$ is the component of $\mathbf{e}_a(\mathbf{e}_b)$ along the crystal axis k, and the integration is restricted to the indium gallium phosphide cross-section (G). During propagation, the relative orientation between the crystal and the propagation direction changes. Both frames can be related through the transformation $((\mathbf{u}_x, \mathbf{u}_y, \mathbf{u}_z) = (\mathbf{u}_\rho\cos(\phi) - \mathbf{u}_\phi\sin(\phi), \mathbf{u}_y, \mathbf{u}_\rho\sin(\phi) + \mathbf{u}_\phi\cos(\phi))$, where $(\mathbf{u}_x, \mathbf{u}_y, \mathbf{u}_z)$ are the vectors of the cartesian basis and $(\mathbf{u}_\rho, \mathbf{u}_y, \mathbf{u}_\phi)$ the cylindrical ones. For simplicity, we limit ourselves to the most efficient processes, i.e., the ones involving a quasi-TE FW mode and a quasi-TM SH mode [21]. Thus, the first and third terms in Eq. (4) can be safely neglected.

The effective nonlinearity can then be expressed as a sum of two Fourier modes: $\kappa(\phi) = \kappa_+e^{i2\phi} + \kappa_-e^{-i2\phi}$ [14], where

$$\kappa_\pm \approx \frac{\omega_0\epsilon_0}{4N_a\sqrt{N_b}}\int_G \chi^{(2)}_{xyz}e_b^{*y}\left(e_a^\rho e_a^\phi \pm i\frac{\left(e_a^\rho\right)^2 + \left(e_a^\phi\right)^2}{2}\right)dS. \tag{5}$$

The values of $\kappa_\pm$ depend on the modal distribution. In Figs. 2(a) and 2(b), the imaginary and real parts of these nonlinear coefficients are plotted as a function of the angle ϕ for two different modes. In Figs. 2(c) and 2(d), we show the coefficients of the Fourier series of $\kappa(\phi)$. In Figs. 2(a) and 2(c), the spatial distribution of the SH is the fundamental TM mode, while in Figs. 2(b) and 2(d) it is the mode TM_{10}. We have calculated $\kappa(\phi)$ by means of the commercial software LUMERICAL MODE SOLUTIONS [23]. The waveguide has a width $w = 1250$ nm, a height $h = 135$ nm, and a bend radius of $R = 15\ \mu$m. The FW wavelength is fixed to 1550 nm. The values of the nonlinear coefficients are $\kappa_+ = -1869i\ \mathrm{W}^{-1/2}\mathrm{m}^{-1}$ and $\kappa_- = 1466i\ \mathrm{W}^{-1/2}\mathrm{m}^{-1}$ when the spatial mode of SH is the TM_{00} and $\kappa_+ = 20i\ \mathrm{W}^{-1/2}\mathrm{m}^{-1}$ and $\kappa_- = 1158i\ \mathrm{W}^{-1/2}\mathrm{m}^{-1}$ when the SH spatial mode is the TM_{10}. It is worth noticing that while in the first case the values of $\kappa_\pm$ are of the same magnitude, when the SH spatial mode is TM_{10}, $\kappa_\pm$ have very different values [13,24].

Next, we have numerically computed $\kappa_\pm$ as a function of the ring radius for the two examples previously considered. Figures 2(e) and 2(f) show $|\kappa_\pm|$ as a function of the waveguide bend radius R for the TM_{00} and TM_{10} modes, respectively. The insets correspond to the Poynting vector of the SH spatial mode with $R = 15\ \mu$m. In the TM_{10} case, $|\kappa_+|$ can be orders of magnitude smaller than $|\kappa_-|$. For radii close to 15 μm, we expect phase mismatched SHG to impact the dynamics. To investigate this regime of cascaded non-linearities, we derive below a mean-field model that includes the phase-mismatched terms.

III. DERIVATION OF THE MODEL

Our starting point is the system of equations Eqs. (3) and the following boundary condition equations:

$$\begin{aligned} a^{(m+1)}(0) &= \sqrt{1-\theta^2}a^{(m)}(2\pi)e^{i\beta_a L} + \theta a_{\mathrm{in}}, \\ b^{(m+1)}(0) &= \sqrt{1-\theta^2}b^{(m)}(2\pi)e^{i\beta_b L}, \end{aligned} \tag{6}$$

where $a^{(m)}, b^{(m)}$ are the field amplitudes at the mth round trip, $|a_{\mathrm{in}}|^2$ is the input power, $L = 2\pi R$ is the resonator length, and θ is the field transmission coefficient of the coupler. These conditions link the output of the mth round trip with the input of the $(m+1)$th one. To further proceed, boundary conditions are injected into the evolution equations. A similar approach has been already employed to generalize the Lugiato-Lefever model of passive fiber cavities [25] and microresonators [26]. This method consists in unfolding the cavity and modeling it as a waveguide with periodic localized gain and losses. Mathematically, these conditions can be expressed by making use of a Dirac delta comb that we include on the right-hand side of Eqs. (3). We expand both propagation constants around the closest resonances: $\beta_{(a,b)} = (2\pi n_{(a,b)} - \delta_{(a,b)})/L$, where $n_{(a,b)}$ are integer numbers. In addition, we perform a phase-rotation $a \to ae^{i\frac{\delta_a}{2\pi}\phi}$, and $b \to be^{i\frac{\delta_b}{2\pi}\phi}$. Therefore, the evolution

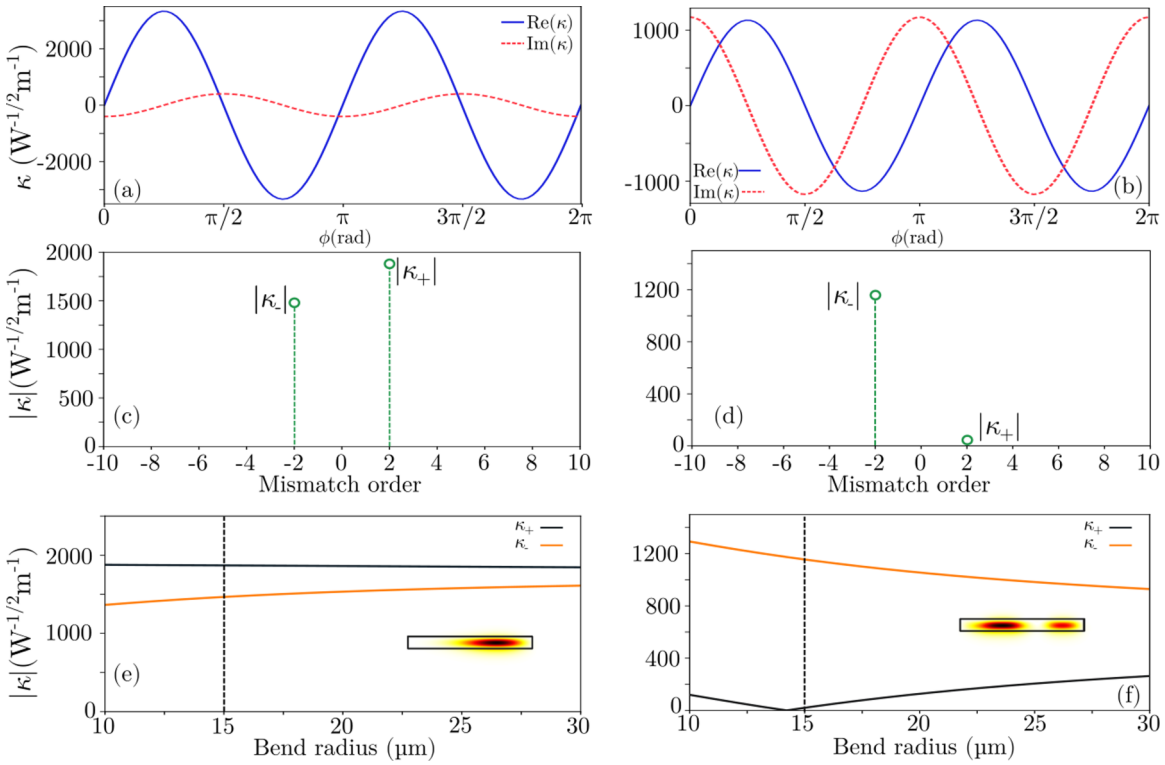

FIG. 2. (a) and (b) show the nonlinear coefficient as a function of ϕ. (a) shows $\kappa(\phi)$ when the SH mode is TM_{00}. (b) shows $\kappa(\phi)$ when the SH mode is TM_{10}. (c) and (d) are the coefficients of the Fourier series of the functions represented in (a) and (b), respectively. (e) and (f) show $|\kappa_+|$ and $|\kappa_-|$ as a function of the bending radius for a SH modes TM_{00} (e) and TM_{10} (f).

equations read

$$
\begin{aligned}
&R^{-1}\frac{da}{d\phi}+\left(i\frac{\delta_a}{L}+\frac{\alpha_a}{2}\right)a-i\kappa^*(\phi)ba^*e^{-i(2n_a-n_b)\phi}\\
&\quad=\left(-\frac{\alpha_c La}{2}+\theta a_{\mathrm{in}}\right)\sum_m\delta(R\phi-mL),\\
&R^{-1}\frac{db}{d\phi}+\left(i\frac{\delta_b}{L}+\frac{\alpha_b}{2}\right)b-i\kappa(\phi)a^2e^{i(2n_a-n_b)\phi}\\
&\quad=-\frac{\alpha_c Lb}{2}\sum_m\delta(R\phi-mL),
\end{aligned}
\tag{7}
$$

where $\alpha_c=\theta^2L^{-1}$. These equations are similar to Eqs. (3), but forced by a Dirac delta comb. The forcing that appears in Eqs. (7) models the periodic gain and losses described by the boundary conditions of the resonator. The Dirac delta comb can be expressed as a Fourier series by making use of the Poisson resummation identity:

$$
\sum_m\delta(R\phi-mL)=\frac{1}{L}\sum_m e^{im\phi}. \tag{8}
$$

Proceeding in this way, and employing Eq. (8), Eqs. (7) become

$$
\begin{aligned}
&R^{-1}\frac{da}{d\phi}+\left(i\frac{\delta_a}{L}+\frac{\alpha_a}{2}\right)a-i\kappa^*(\phi)ba^*e^{-i(2n_a-n_b)\phi}\\
&\quad\times\left(-\frac{\alpha_c a}{2}+\frac{\theta}{L}a_{\mathrm{in}}\right)\sum_m e^{im\phi}\\
&\quad=R^{-1}\frac{db}{d\phi}+\left(i\frac{\delta_b}{L}+\frac{\alpha_b}{2}\right)b-i\kappa(\phi)a^2e^{i(2n_a-n_b)\phi}\\
&\quad=-\frac{\alpha_c b}{2}\sum_m e^{im\phi}.
\end{aligned}
\tag{9}
$$

Without loss of generality, the process involving κ_+ is considered to be quasi-phase-matched, i.e., $2n_a-n_b=-2$. However, the results that we will obtain can be easily generalized to $2n_a-n_b=2$ or for any poled resonator where QPM is verified. Thus, the evolution equations become

$$
\begin{aligned}
&R^{-1}\frac{da}{d\phi}+\left(i\frac{\delta_a}{L}+\frac{\alpha_p}{2}\right)a-i(\kappa_+^*+\kappa_-^*e^{+i4\phi})ba^*\\
&\quad=\left(-\frac{\alpha_c a}{2}+\frac{\theta}{L}a_{\mathrm{in}}\right)\sum_m e^{im\phi},\\
&R^{-1}\frac{db}{d\phi}+\left(i\frac{\delta_b}{L}+\frac{\alpha_p}{2}\right)b-i(\kappa_++\kappa_-e^{-i4\phi})a^2\\
&\quad=-\frac{\alpha_c b}{2}\sum_m e^{im\phi}.
\end{aligned}
\tag{10}
$$

The detunings δ_a and δ_b are linked through the relation $\delta_b=2\delta_a=2\delta_0$ if $\Delta\beta=-2R^{-1}$. As a first-order approximation, we can neglect complex exponentials on the left-hand side of Eqs. (10). However, this simplification, also known as the fast-rotating wave (FRW) approximation, may not be valid for large values of $|\kappa_-|$. To derive a model that also describes the regimes where κ_- has a non-negligible contribution, we employ the averaging method described in

Ref. [27]. We express $a(\phi)$ and $b(\phi)$ as Fourier series $(a, b) = \sum_k (a_k(\phi), b_k(\phi))e^{ik\phi}$, where each coefficient k relates to the longitudinal mode N of the cavity as $N_{a,b} = n_{a,b} + k$, and substitute them in Eqs. (10). Then, by collecting the terms that oscillate at the same frequency, considering critical coupling, and equal loss for both modes $\alpha_c = \alpha_a = \alpha_b = \alpha$, we find

$$\begin{aligned}
&\frac{dA_k}{d\bar{\phi}} + \left(i(\Delta + 2\mathcal{F}k) + \frac{1}{2}\right)A_k \\
&\quad - i\sum_m \left(\frac{\kappa_-^*}{\kappa_+^*}A^*_{m+4-k}B_m + A^*_{m-k}B_m\right) \\
&\quad = -\frac{1}{2}\sum_m A_m + \rho, \\
&\frac{dB_k}{d\bar{\phi}} + \left(2i(\Delta + \mathcal{F}k) + \frac{1}{2}\right)B_k \\
&\quad - i\sum_m \left(\frac{\kappa_-}{\kappa_+}A_{k+4-m}A_m + A_{m-k}A_m\right) \\
&\quad = -\frac{1}{2}\sum_m B_m,
\end{aligned} \tag{11}$$

where we introduced the finesse $\mathcal{F} = \pi(\alpha L)^{-1}$ and the following normalization: $\Delta = \delta\alpha L^{-1}$, $\rho = \kappa_+ L a_{\text{in}}(\mathcal{F}/\pi)^{3/2}$, $(A_k, B_k) = \alpha\kappa_+^{-1}(a_k, b_k)$, $\bar{\phi} = R\alpha^{-1}\phi$. We now have a system of equations for each longitudinal mode of the cavity. These modes interact via the nonlinear terms and the periodic losses induced by the coupling with the bus waveguide. In this expansion, the order $k = 0$ represents the averaged dynamics over one round trip. Note that all the coefficients of the system do not have the same order of magnitude, while Δ and ρ are close to 1, $\mathcal{F}$ may reach values of hundreds for high-finesse resonators. This difference allows us to make use of a multiscale expansion when $k \neq 0$. By writing $(A_k, B_k) = \sum_l (A_k^{(l)}, B_k^{(l)})\epsilon^l$, where the multiscale parameter is $\epsilon = \mathcal{F}^{-1}$, an infinite hierarchy of algebraic equations is obtained:

$$\epsilon^{-1} : A_{-4}^{(0)} = 0\,, \quad B_4^{(0)} = 0, \tag{12}$$

$$\begin{aligned}
\epsilon^0 : A_4^{(1)} &= \frac{1}{8}\left(\frac{\kappa_-^*}{\kappa_+^*}A_0^* B_0 + \left(\rho - \frac{A_0}{2}\right)\right), \\
B_{-4}^{(1)} &= -\frac{1}{8}\left(\frac{\kappa_-}{\kappa_+}A_0^2 + \frac{B_0}{2}\right),
\end{aligned} \tag{13}$$

where we only show the cases where there is a coupling with the order $k = 0$ at ϵ^0. For low values of ρ and high values of $|\kappa_-/\kappa_+|$, we can make the approximation

$$A_4^{(1)} = \frac{\kappa_-^*}{8\kappa_+^*}A_0^* B_0, \quad B_{-4}^{(1)} = -\frac{\kappa_-}{8\kappa_+}A_0^2. \tag{14}$$

These equations relate the longitudinal mode $k = 0$ with the modes $k = \pm 4$. Therefore, the evolution of the dimensional fields $a(\phi)$ and $b(\phi)$ can be expressed as

$$\begin{aligned}
a(\phi) &= a_0 + \frac{\kappa_-^* R}{4}a_0^* b_0 e^{i4\phi}, \\
b(\phi) &= b_0 - \frac{\kappa_- R}{4}a_0^2 e^{-i4\phi},
\end{aligned} \tag{15}$$

where a_0 and b_0 are governed by the following differential equations:

$$\begin{aligned}
&R^{-1}\frac{da_0}{d\phi} + \left(i\frac{\delta_0}{L} + \alpha\right)a_0 - i\kappa_+^* b_0 a_0^* \\
&\quad - i\gamma(|a_0|^2 - |b_0|^2)a_0 = \frac{\theta}{L}a_{\text{in}}, \\
&R^{-1}\frac{db_0}{d\phi} + \left(i\frac{2\delta_0}{L} + \alpha\right)b_0 - i\kappa_+ a_0^2 + 2i\gamma|a_0|^2 b_0 = 0,
\end{aligned} \tag{16}$$

with $\gamma = -|\kappa_-|^2 L/(8\pi)$. Interestingly, higher-order wave-mixing terms, akin to a third-order nonlinearity, appear in Eqs. (16). Note that this nonlinearity does not exactly correspond to a pure Kerr interaction, since there is no self-phase modulation term in the second equation. In addition, the self- and cross-phase modulation terms in the first equation are of opposite signs. The magnitude of the third-order nonlinearity corresponds to the well-known cascading limit, which is $\gamma = |\kappa_-|^2/(2\Delta\beta)$ [15].

To see the effect of phase-mismatched terms and compare results to the outcome of a model where the FRW approximation is used, we performed some numerical simulations. We considered a resonator with $\mathcal{F} = 300$, pumped in the TE_{00} mode with $|a_{\text{in}}|^2 = 200$ mW. We supposed a critically coupled resonator. The dimensions of the resonator were chosen such that the process involving κ_+ verified QPM at $\lambda_p = 1550$ nm with the SH spatial mode TM_{10}: $h = 130$ nm, $w = 1250$ nm and $R = 14.5$ μm. With these values, we find $\kappa_+ = 38i$ $\text{W}^{-1/2}\text{m}^{-1}$ and $\kappa_- = 1101i$ $\text{W}^{-1/2}\text{m}^{-1}$. Furthermore, here we chose a normalized detuning $\Delta = -0.4$. In Figs. 3(a) and 3(b), we show the intracavity power evolution of the FW and SH fields. The dark solid line corresponds to the map, Eqs. (3) and (6). The fast oscillations are due to the phase-mismatched terms and are clearly appreciable in the insets. The blue dashed-dotted line corresponds to Eqs. (16) after applying the FRW approximation, i.e., setting $\gamma = 0$. From the figure, it is clear that the FRW approximation is not valid in the considered regime because the mean value of the stationary states is significantly different. The green dashed line is the numerical solution of Eqs. (16). In the insets of Fig. 3, we display a zoom of the last round trips. The result obtained through Eqs. (15) are plotted in dashed red in Fig. 3(a) and in dashed magenta in Fig. 3(b). The numerical results are shown in black for comparison. The value of a_0 and b_0 employed in the analytical expression is obtained from the averaged value of the fields over one round trip. We can see that both curves are nearly superimposed. We find excellent agreement between our model and the map Eqs. (3) and (6), validating the use of a mean-field equation to describe the competition between the phase-matched terms, driving the frequency conversion, and an effective Kerr nonlinearity imposed by the phase-mismatched terms.

IV. STATIONARY SOLUTIONS

Next, we analyze the impact of the phase-mismatched terms on the stationary solutions of the system. In normalized

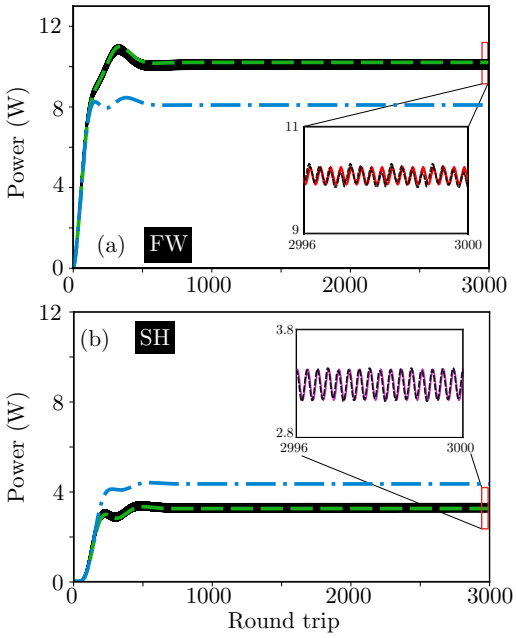

FIG. 3. Evolution of power in the FW (a) and SH (b) modes. Black (solid) line corresponds to the map, blue (point-dashed) line corresponds to Eqs. (16) with $\gamma = 0$, and green (dashed) line is the solution of Eqs. (16) with $\gamma \neq 0$. The parameters are $\Delta = -0.4$, $|a_{\rm in}|^2 = 0.2$ W, $|\kappa_+| = 38$ W$^{-1/2}$m^{-1}, $|\kappa_-| = 1101$ W$^{-1/2}$m^{-1}, $R = 14.5$ μm.

form, Eqs. (16) read

$$\frac{dA_0}{d\bar{\phi}} + (1 + i\Delta)A_0 - i(\bar{\gamma}(|A_0|^2 - |B_0|^2)A_0 + B_0A^*) = \rho,$$
$$\frac{dB_0}{d\bar{\phi}} + (1 + i2\Delta)B_0 - i\left(A_0^2 - 2\bar{\gamma}|A_0|^2B_0\right) = 0, \tag{17}$$

where $\bar{\gamma} = \text{sign}(\Delta\beta)|\kappa_-|^2/(8|\kappa_+|^2\mathcal{F})$. The normalized coefficient $\bar{\gamma}$ shows the relevance of phase-mismatched terms. Note that $\bar{\gamma}$ has a non-negligible value when $|\kappa_\pm|$ have different orders of magnitude. More precisely, the coefficient $\bar{\gamma}$ confirms that mismatched terms are relevant when $|\kappa_-| \gg |\kappa_+|$. To study the impact of $\bar{\gamma}$ and verify the validity of the mean-field equations for different values of the detuning, we compared the steady-state solutions obtained with the map and with Eqs. (17). To get rid of eventual oscillations of the map solutions, we calculated the mean value of the intensity over one round trip. The stationary states of Eqs. (17) were found by imposing $\dot{A} = \dot{B} = 0$ and making use of numerical continuation by means of the free distribution program AUTO [28]. The value of $|a_{\rm in}|$ is chosen such that ρ is equal to 2.34 in both cases. This value of ρ is below the threshold for bistablity and self-pulsing [29]. The resonator dimensions are chosen so SH generation is quasi-phase-matched at $\lambda_p = 1550$ nm with $R = 15.25$ μm and $w = 1250$ nm. The finesse is set to $\mathcal{F} = 300$.

The first case corresponds to a resonator where QPM is verified for the TM$_{00}$ mode. The value of the height is $h = 122$ nm. The values of the nonlinear coefficients are $\kappa_+ = 1613i$ W$^{-1/2}$m^{-1} and $\kappa_- = 1305i$ W$^{-1/2}$m^{-1}. The value of $\bar{\gamma} = -3 \times 10^{-4}$ and, thus, the impact of mismatched terms is negligible. The intracavity power of the steady states as a function of Δ is displayed in Fig. 4(a). Within this limit, resonances are symmetric with respect to the detuning and the maximum of intracavity power for SH is found for zero detuning [30,31].

Next, we studied the case where the SH propagates in a TM$_{10}$ mode. The height is $h = 130$ nm. The values of the nonlinear coefficients are $\kappa_+ = 57i$ W$^{-1/2}$m^{-1} and $\kappa_- = 1083i$ W$^{-1/2}$m^{-1}. In this case, $\bar{\gamma} = -0.16$, the impact of cascaded nonlinearities can be clearly seen on the resonances. They become asymmetric, akin to those found when the Kerr nonlinearity is included [30].

We stress that the two configurations shown in Fig. 4 are very different. The conversion is much weaker in the latter case because the resonator is engineered such that the weaker nonlinear mode (κ_+) is quasi-phase-matched so as to maximize the impact of cascaded nonlinearities. This difference can be appreciated by calculating the conversion efficiency ($\eta = \theta|b_{\rm max}|^2/|a_{\rm in}|^4$) for the two configurations. It is as high as $\eta = 970,000$ %/W in the first case, which is of the same order of magnitude as the state of the art [6]. However, in the other case, we find a significantly lower conversion efficiency of $\eta = 1,150$ %/W.

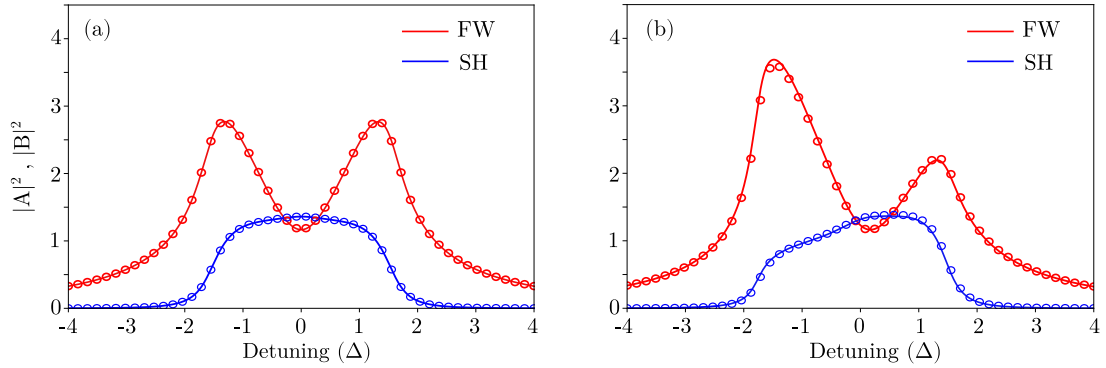

FIG. 4. Comparison between the steady states obtained with the exact map (circles) and the averaged equations Eqs. (17) (blue line for SH and red line for the FW). (a) The phase-matched term mode is TM$_{00}$. Coefficients are $\kappa_- = 1305$i W$^{-1/2}$m^{-1}, $\kappa_+ = -1613i$ W$^{-1/2}$m^{-1}, $\bar{\gamma} = -3 \times 10^{-4}$ and $h = 122$ nm. (b) The phase-matched mode is TM$_{10}$. Coefficients are $\kappa_- = 1083$i W$^{-1/2}$ m^{-1}, κ_+=57i W$^{-1/2}$m^{-1}, $\bar{\gamma} = -0.16$ and $h = 130$ nm.

Our results hence suggest that the impact of cascaded nonlinearities is negligible as long as the larger nonlinear mode is quasi-phase-matched, as indicated from the normalized parameter $\bar{\gamma} = \text{sign}(\Delta\beta)|\kappa_-|^2/(8|\kappa_+|^2\mathcal{F})$. Yet we showed that modal phase matching allows us to engineer competing nonlinearities, and expect the mismatched terms to have a significant impact on the known oscillatory and modulation instabilities arising in cavity-enhanced SH generation [29,32].

V. CONCLUSIONS

We have analyzed quasi-phase-matched SH generation in a ring resonator made of a semiconductor with zinc-blende structure, and hence a $\bar{4}$3m symmetry. Starting from the boundary conditions and propagation equations, we derived a mean-field model that takes into account the phase-mismatched processes. We showed that they act as an effective third-order nonlinearity which plays a fundamental role for certain configurations. Our analysis can readily be generalized to resonators made of poled materials.

ACKNOWLEDGMENTS

This work was supported by funding from the European Research Council (ERC) under the European Union's Horizon 2020 research and innovation program (Grant Agreement No. 757800). P.P.-R. acknowledges support from the Fonds de la Recherche Scientifique F.R.S.-FNRS.

[1] M. M. Fejer, Nonlinear optical frequency conversion, Phys. Today **47**(5), 25 (1994).
[2] W. Petrich, Mid-infrared and raman spectroscopy for medical diagnostics, Appl. Spectrosc. Rev. **36**, 181 (2001).
[3] J.-W. Pan, Z.-B. Chen, C.-Y. Lu, H. Weinfurter, A. Zeilinger, and M. Żukowski, Multiphoton entanglement and interferometry, Rev. Mod. Phys. **84**, 777 (2012).
[4] C. Wang, C. Langrock, A. Marandi, M. Jankowski, M. Zhang, B. Desiatov, M. M. Fejer, and M. Lonar, Ultrahigh-efficiency wavelength conversion in nanophotonic periodically poled lithium niobate waveguides, Optica **5**, 1438 (2018).
[5] L. Chang, A. Boes, X. Guo, D. T. Spencer, M. J. Kennedy, J. D. Peters, N. Volet, J. Chiles, A. Kowligy, N. Nader, D. D. Hickstein, E. J. Stanton, S. A. Diddams, S. B. Papp, and J. E. Bowers, Heterogeneously integrated GaAs waveguides on insulator for efficient frequency conversion, Laser Photonics Rev. **12**, 1800149 (2018).
[6] J. Lu, J. B. Surya, X. Liu, A. W. Bruch, Z. Gong, Y. Xu, and H. X. Tang, Periodically poled thin-film lithium niobate microring resonators with a second-harmonic generation efficiency of 250, 000%/w, Optica **6**, 1455 (2019).
[7] R. Boyd, *Nonlinear Optics*, 3rd ed. (Elsevier, USA, 2008).
[8] V. S. Ilchenko, A. A. Savchenkov, A. B. Matsko, and L. Maleki, Nonlinear Optics and Crystalline Whispering Gallery Mode Cavities, Phys. Rev. Lett. **92**, 043903 (2004).
[9] J.-Y. Chen, Z.-H. Ma, Y. M. Sua, Z. Li, C. Tang, and Y.-P. Huang, Ultra-efficient frequency conversion in quasi-phase-matched lithium niobate microrings, Optica **6**, 1244 (2019).
[10] L. A. Eyres, P. J. Tourreau, T. J. Pinguet, C. B. Ebert, J. S. Harris, M. M. Fejer, L. Becouarn, B. Gerard, and E. Lallier, All-epitaxial fabrication of thick, orientation-patterned GaAs films for nonlinear optical frequency conversion, Appl. Phys. Lett. **79**, 904 (2001).
[11] G. Lin, J. U. Fürst, D. V. Strekalov, and N. Yu, Wide-range cyclic phase matching and second harmonic generation in whispering gallery resonators, Appl. Phys. Lett. **103**, 181107 (2013).
[12] G. Lin, A. Coillet, and Y. K. Chembo, Nonlinear photonics with high-Q whispering-gallery-mode resonators, Adv. Opt. Photonics **9**, 828 (2017).
[13] Y. Dumeige and P. Féron, Whispering-gallery-mode analysis of phase-matched doubly resonant second-harmonic generation, Phys. Rev. A **74**, 063804 (2006).
[14] P. S. Kuo, W. Fang, and G. S. Solomon, $\bar{4}$-quasi-phase-matched interactions in GaAs microdisk cavities, Opt. Lett. **34**, 3580 (2009).
[15] C. B. Clausen, O. Bang, and Y. S. Kivshar, Spatial Solitons and Induced Kerr Effects in Quasi-p-Matched Quadratic Media, Phys. Rev. Lett. **78**, 4749 (1997).
[16] R. DeSalvo, H. Vanherzeele, D. J. Hagan, M. Sheik-Bahae, G. Stegeman, and E. W. Van Stryland, Self-focusing and self-defocusing by cascaded second-order effects in KTP, Opt. Lett. **17**, 28 (1992).
[17] O. Bang, C. B. Clausen, P. L. Christiansen, and L. Torner, Engineering competing nonlinearities, Opt. Lett. **24**, 1413 (1999).
[18] B. B. Zhou, A. Chong, F. W. Wise, and M. Bache, Ultrafast and Octave-Spanning Optical Nonlinearities from Strongly Phase-Mismatched Quadratic Interactions, Phys. Rev. Lett. **109**, 043902 (2012).
[19] M. Levenius, M. Conforti, F. Baronio, V. Pasiskevicius, F. Laurell, C. De Angelis, and K. Gallo, Multistep quadratic cascading in broadband optical parametric generation, Opt. Lett. **37**, 1727 (2012).
[20] N. Poulvellarie, U. Dave, K. Alexander, C. Ciret, M. Billet, C. Mas Arabi, F. Raineri, S. Combrie, A. D. Rossi, G. Roelkens, S.-P. Gorza, B. Kuyken, and F. Leo, Second harmonic generation enabled by longitudinal electric field components in photonic wire waveguides, arXiv:2001.01709.
[21] C. Ciret, K. Alexander, N. Poulvellarie, M. Billet, C. Mas Arabi, B. Kuyken, S.-P. Gorza, and F. Leo, Full vectorial modeling of second harmonic generation in III-V-on-insulator nanowires, arXiv:2001.02210.
[22] Y. Ueno, V. Ricci, and G. I. Stegeman, Second-order susceptibility of $Ga_{0.5}In_{0.5}P$ crystals at 1.5 μm and their feasibility for waveguide quasi-phase matching, J. Opt. Soc. Am. B **14**, 1428 (1997).
[23] https://www.lumerical.com/products/mode.
[24] P. S. Kuo, J. Bravo-Abad, and G. S. Solomon, Second-harmonic generation using $\bar{4}$-quasi-phasematching in a GaAs whispering-gallery-mode microcavity, Nat. Commun. **5**, 3109 (2014).
[25] M. Conforti and F. Biancalana, Multi-resonant Lugiato-Lefever model, Opt. Lett. **42**, 3666 (2017).
[26] X. Xue, F. Leo, Y. Xuan, J. A. Jaramillo-Villegas, P.-H. Wang, D. E. Leaird, M. Erkintalo, M. Qi, and A. M. Weiner, Second-harmonic-assisted four-wave mixing in chip-based

microresonator frequency comb generation, Light: Sci. Appl. **6**, e16253 (2017).

[27] Y. S. Kivshar, N. Grønbech-Jensen, and R. D. Parmentier, Kinks in the presence of rapidly varying perturbations, Phys. Rev. E **49**, 4542 (1994).

[28] E. J. Doedel, T. F. Fairgrieve, B. Sandstede, A. R. Champneys, Y. A. Kuznetsov, and X. Wang, Auto-07p: Continuation and bifurcation software for ordinary differential equations (2007), http://indy.cs.concordia.ca/auto/.

[29] P. Drummond, K. McNeil, and D. Walls, Non-equilibrium transitions in sub/second harmonic generation, Opt. Acta: Int. J. Opt. **27**, 321 (1980).

[30] A. Villois and D. V. Skryabin, Soliton and quasi-soliton frequency combs due to second harmonic generation in microresonators, Opt. Express **27**, 7098 (2019).

[31] T. Hansson, P. Parra-Rivas, M. Bernard, F. Leo, L. Gelens, and S. Wabnitz, Quadratic soliton combs in doubly-resonant second-harmonic generation, Opt. Lett. **43**, 6033 (2018).

[32] F. Leo, T. Hansson, I. Ricciardi, M. De Rosa, S. Coen, S. Wabnitz, and M. Erkintalo, Walk-Off-Induced Modulation Instability, Temporal Pattern Formation, and Frequency Comb Generation in Cavity-Enhanced Second-Harmonic Generation, Phys. Rev. Lett. **116**, 033901 (2016).